

Radiation-Driven Warping of Circumbinary Disks Around Eccentric Young Star Binaries

Kimitake HAYASAKI¹, Bong Won SOHN^{1,2}, Atsuo T. OKAZAKI³, Taehyun JUNG¹,
Guangyao ZHAO¹, and Tsuguya NAITO⁴

kimi@kasi.re.kr

Received _____; accepted _____

¹Korea Astronomy and Space Science Institute, Daedeokdaero 776, Yuseong, Daejeon 305-348, Korea

²Department of Astronomy and Space Science, University of Science and Technology, 217 Gajeong-ro, Daejeon, Korea

³Faculty of Engineering, Hokkai-Gakuen University, Toyohira-ku, Sapporo 062-8605, Japan

⁴Faculty of Management Information, Yamanashi Gakuin University, Kofu, Yamanashi 400-8575, Japan

ABSTRACT

We study a warping instability of a geometrically thin, non-self-gravitating, circumbinary disk around young binary stars on an eccentric orbit. Such a disk is subject to both the tidal torques due to a time-dependent binary potential and the radiative torques due to radiation emitted from each star. The tilt angle between the circumbinary disk plane and the binary orbital plane is assumed to be very small. We find that there is a radius within/beyond which the circumbinary disk is unstable to radiation-driven warping, depending on the disk density and temperature gradient indices. This marginally stable warping radius is very sensitive to viscosity parameters, a fiducial disk radius and the temperature measured there, the stellar luminosity, and the disk surface density at a radius where the disk changes from the optically thick to thin for the irradiation from the central stars. On the other hand, it is insensitive to the orbital eccentricity and binary irradiation parameter, which is a function of the binary mass ratio and luminosity of each star. Since the tidal torques can suppress the warping in the inner part of the circumbinary disk, the disk starts to be warped in the outer part. While the circumbinary disks are most likely to be subject to the radiation-driven warping on a AU to kilo-AU scale for binaries with young massive stars more luminous than $10^4 L_{\odot}$, the radiation driven warping does not work for those around young binaries with the luminosity comparable to the solar luminosity.

Subject headings: accretion, accretion disks - hydrodynamics - masers - protoplanetary disks - stars: massive - stars: low-mass - stars: formation - (stars:) binaries: general

1. Introduction

About 60% of main sequence stars are considered to be born as binary or multiple systems (Duquennoy & Mayor 1991). Indeed, the direct imaging of the circumbinary disk was successfully done for a few young binary star systems with the binary mass comparable to a solar mass, including GG Tau (Dutrey et al. 1994) and UY Aurigae (Duvert et al. 1998) by the Plateau de Bure Interferometer (PdBI). It is confirmed by numerical simulations that the circumbinary disk is formed around such young low mass binary stars embedded in the dense molecular gas (Artymowicz & Lubow 1994; Bate & Bonnell 1997; Günther & Kley 2002, 2004).

The existence of a significant number of OB eclipsing binaries (Hilditch et al. 2005) suggests that most known massive stars are also born as binary or multiple systems (Sana et al. 2012). Such binaries are expected to be accompanied by circumbinary disks at the early stage of the massive star formation. Contrary to the case of T Tauri stars, however, the massive star formation is still poorly understood because the observation of massive star forming regions is challenging. This is because they are obscured by a dusty environment and the chance to observe massive young stellar objects is small because of their short lives. Araya et al. (2010) suggested that observed periodic maser emissions are originated from periodic accretion onto the binary stars on a significantly eccentric orbit from the circumbinary disk (Artymowicz & Lubow 1996), although there are two other scenarios: the colliding wind binary scenario (van der Walt 2011) and the scenario of pulsation of protostars growing via high mass accretion rate (Inayoshi et al. 2013).

It is natural that the circumstellar and circumbinary disks in the star forming regions have a warped structure. Krist et al. (2005) suggested that there is observational evidence for the disk warping in GG Tau system. The tidal effects of close encounters between stars and a disk surrounding it can make the disk outer parts misaligned or warped

(Moeckel&Bally 2006). If the circumbinary disk is originally misaligned with the binary orbital plane, it should be warped by the tidal alignment, although the disk tilt secularly decays by the disk viscosity (Facchini et al. 2013; Lodato&Facchini 2013). The origin of the misalignment and disk warping is, however, still a matter of debate.

Hayasaki et al. (2014a) (hereafter, Paper I) derived the condition that a circumbinary disk subject to both the tidal torque and the torque due to the radiation emitted from two accretion disks around the individual supermassive black holes is unstable to the radiation-driven warping in the context of observed warped maser disks in active galactic nuclei (e.g., Kuo et al. 2011; Kormendy&Ho 2013). They assumed that the binary is on a circular orbit and the irradiation luminosity is proportional to the mass accretion rate. There is, however, observational evidence that young binaries have a significant orbital eccentricity (Mathieu et al. 1990). In addition, the circumbinary disk is mainly irradiated by two young stars in a binary in the current problem. In order to apply our previous model to those binaries, therefore, we need to relax the above assumptions adopted in Paper I and make the binary mass scale down to the stellar mass from supermassive black hole mass.

In this paper, we study the warping instability of a circumbinary disk around young binary stars on an eccentric orbit. In section 2, we describe the external torques acting on a circumbinary disk. We consider both the tidal torques originating from a time-dependent binary potential and the radiative torques from the binary stars. In section 3, we examine the evolution of a slightly tilted circumbinary disk subject to those two torques, and derive the warping condition and timescale of the local precession of the linear warping mode. Finally, section 4 is devoted to summary and discussion of our scenario.

2. External Torques acting on the circumbinary disk

Let us consider the torques from the binary potential acting on the circumbinary disk surrounding two stars in a binary on an eccentric orbit. Figure 1 illustrates a schematic picture of the setting of our model; binary stars orbiting each other are surrounded by a misaligned circumbinary disk. The binary is put on the x - y plane with its center of mass being at the origin in the Cartesian coordinate. The masses of the primary and secondary stars are represented by M_1 and M_2 , respectively, and $M = M_1 + M_2$. We put a circumbinary disk around the origin. The unit vector of specific angular momentum of the circumbinary disk is expressed by (e.g. Pringle 1996)

$$\mathbf{l} = \cos \gamma \sin \beta \mathbf{i} + \sin \gamma \sin \beta \mathbf{j} + \cos \beta \mathbf{k}, \quad (1)$$

where β is the tilt angle between the circumbinary disk plane and the binary orbital plane, and γ is the azimuth of tilt. Here, \mathbf{i} , \mathbf{j} , and \mathbf{k} are unit vectors in the x , y , and z , respectively. The position vector of the circumbinary disk can be expressed by

$$\mathbf{r} = r(\cos \phi \sin \gamma + \sin \phi \cos \gamma \cos \beta) \mathbf{i} + r(\sin \phi \sin \gamma \cos \beta - \cos \phi \cos \gamma) \mathbf{j} - r \sin \phi \sin \beta \mathbf{k} \quad (2)$$

where the azimuthal angle ϕ is measured from the descending node. The only difference from the Paper I is the position vector of each star, which is given by

$$\mathbf{r}_i = r_i \cos f_i \mathbf{i} + r_i \sin f_i \mathbf{j} \quad (i = 1, 2), \quad (3)$$

where $f_2 = f_1 + \pi$ is the true anomaly and r_i is written as

$$r_i = \xi_i \frac{a(1 - e^2)}{1 + e \cos f_i} \quad (4)$$

with $\xi_1 \equiv q/(1 + q)$ and $\xi_2 \equiv 1/(1 + q)$. Here, e is the binary orbital eccentricity, $q = M_2/M_1$ is the binary mass ratio, and $a = a_1 + a_2$ is the binary semi-major axis with $a_1 \equiv \xi_1 a$ and $a_2 \equiv \xi_2 a$. These and other model parameters are listed in Table 1.

Table 1: Model parameters

Definition	Symbol
Total stellar mass	M
Primary stellar mass	M_1
Secondary stellar mass	M_2
Binary mass ratio	$q = M_2/M_1$
Mass ratio parameters	$\xi_1 = q/(1 + q), \xi_2 = 1/(1 + q)$
Binary semi-major axis	a
Orbital eccentricity	e
Orbital frequency	$\Omega_{\text{orb}} = \sqrt{GM/a^3}$
Orbital period	$P_{\text{orb}} = 2\pi/\Omega_{\text{orb}}$
True anomaly	$f_2 = f_1 + \pi$
Tilt angle	β
Azimuth of tilt	γ
Azimuthal angle	ϕ
Shakura-Sunyaev viscosity parameter	α
Horizontal shear viscosity	ν_1
Vertical shear viscosity	ν_2
Ratio of vertical to horizontal shear viscosities	$\eta = \nu_2/\nu_1$
Luminosities emitted from two stars in a binary	L_1, L_2
Total luminosity	$L = L_1 + L_2$
Binary irradiation parameter	$\zeta = (\xi_1^2 L_1 + \xi_2^2 L_2)/L$

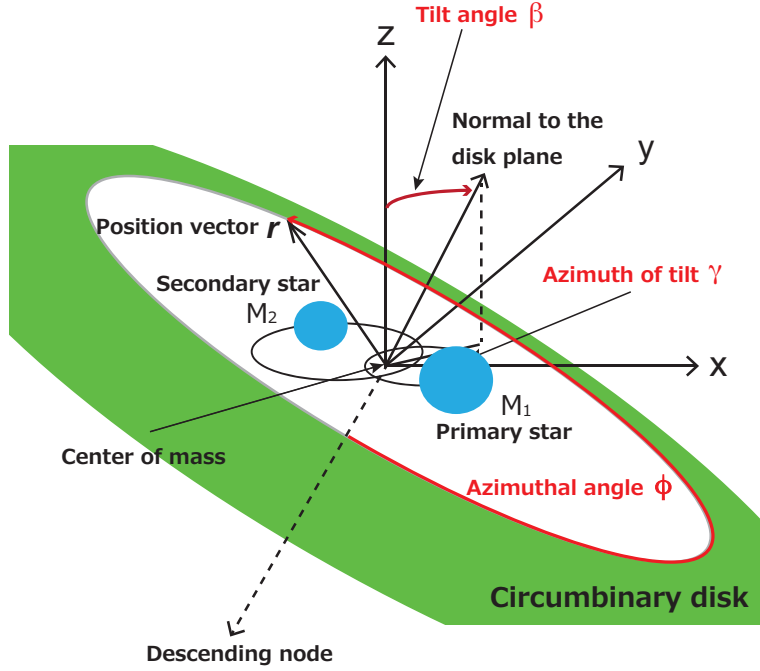


Fig. 1.— Configuration of a young binary star system composed of two stars and a circumbinary disk surrounding them. There are two angles (β, γ) which specify the orientation of the circumbinary disk plane with respect to the binary orbital plane (x - y plane). The azimuthal angle (ϕ) of an arbitrary position on the circumbinary disk is measured from the descending node.

2.1. Gravitational Torques

The gravitational force on the unit mass at position \mathbf{r} on the circumbinary disk can be written by

$$\mathbf{F}_{\text{grav}} = - \sum_{i=1}^2 \frac{GM_i}{|\mathbf{r} - \mathbf{r}_i|^3} (\mathbf{r} - \mathbf{r}_i) \quad (5)$$

The corresponding torque is given by

$$\mathbf{t}_{\text{grav}} = \mathbf{r} \times \mathbf{F}_{\text{grav}} = \sum_{i=1}^2 \frac{GM_i}{|\mathbf{r} - \mathbf{r}_i|^3} (\mathbf{r} \times \mathbf{r}_i) \quad (6)$$

We consider the tidal warping/precession with timescales much longer than local rotation period of the circumbinary disk. This allows us to use the torque averaged in the azimuthal direction and over the orbital period:

$$\begin{aligned} \langle \mathbf{T}_{\text{grav}} \rangle &\approx \frac{1}{4\pi^2} \int_0^{2\pi} \int_0^{2\pi} \mathbf{t}_{\text{grav}} d\phi d(\Omega_{\text{orb}}t) = \frac{3}{8} \xi_1 \xi_2 \left(\frac{a}{r}\right)^2 \frac{GM}{r} \\ &\times \left[(1 - e^2) \sin \gamma \sin 2\beta \mathbf{i} - (1 + 4e^2) \cos \gamma \sin 2\beta \mathbf{j} + 5e^2 \sin 2\gamma \sin^2 \beta \mathbf{k} \right], \end{aligned} \quad (7)$$

where $\Omega_{\text{orb}} = \sqrt{GM/a^3}$ is the angular frequency of mean binary motion. Here, we used for the integration the following relationship:

$$d(\Omega_{\text{orb}}t) = \frac{(1 - e^2)^{3/2}}{(1 + e \cos f_i)^2} df \quad (8)$$

and the approximations:

$$\begin{aligned} |\mathbf{r} - \mathbf{r}_i|^{-3} &\approx r^{-3} \left[1 + 3 \frac{\mathbf{r} \cdot \mathbf{r}_i}{r^2} + \mathcal{O}((r_i/r)^2) \right], \\ (1 + e \cos f_i)^{-4} &\approx 1 - 4e \cos f_i + 10e^2 \cos^2 f_i + \mathcal{O}(e^3). \end{aligned} \quad (9)$$

Note that equation (7) is derived in the same manner as in equation (7) of Hayasaki et al. (2014b).

For a small tilt angle $\beta \ll 1$, equation (7) is reduced to

$$\langle \mathbf{T}_{\text{grav}} \rangle \approx \frac{3}{4} \xi_1 \xi_2 \left(\frac{a}{r}\right)^2 \frac{GM}{r} \left[(1 - e^2) l_y \mathbf{i} - (1 + 4e^2) l_x \mathbf{j} \right], \quad (10)$$

where l_x and l_y can be written from equation (1) as $l_x = \beta \cos \gamma$ and $l_y = \beta \sin \gamma$. The magnitude of the specific tidal torque with $\beta \ll 1$ is then given by

$$|\langle \mathbf{T}_{\text{grav}} \rangle| = \frac{3}{4} \xi_1 \xi_2 \left(\frac{a}{r}\right)^2 \frac{GM}{r} \beta \sqrt{5e^2(3e^2 + 2) \cos^2 \gamma + (e^2 - 1)^2}. \quad (11)$$

The tidal torque tends to align the tilted circumbinary disk with the orbital plane (c.f. Bate et al. 2000). The tidal alignment timescale for $\beta \ll 1$ is given by

$$\tau_{\text{tid}} = \frac{|\mathbf{J}| \sin \beta}{|\langle \mathbf{T}_{\text{grav}} \rangle|} \approx \frac{8}{3\pi} \frac{1}{\sqrt{5e^2(3e^2 + 2) \cos^2 \gamma + (e^2 - 1)^2}} \left(\frac{1/4}{\xi_1 \xi_2}\right) \left(\frac{r}{a}\right)^{7/2} P_{\text{orb}}, \quad (12)$$

where $\mathbf{J} \equiv r^2\Omega\mathbf{l}$ with the disk angular frequency $\Omega = \sqrt{GM/r^3}$ and $P_{\text{orb}} = 2\pi/\Omega_{\text{orb}}$ are the specific angular momentum and binary orbital period, respectively. Equation (12) is reduced to equation (8) of Paper I for $e = 0$. Note that the tidal alignment timescale depends on the azimuth of tilt for $e \neq 0$. Since the inner edge of the circumbinary disk is estimated to be $\sim 2a$ (Artymowicz & Lubow 1994), the tidal alignment timescale is longer than the binary orbital period.

2.2. Radiative Torques

The circumbinary disk around young binary stars can be mainly illuminated by light emitted from each star. The re-radiation from the circumbinary-disk surface, which absorbs photons emitted from these stars, causes a reaction force. This is the origin of the radiative torques. Here, the central two stars are can be regarded as point irradiation sources, because each star is much smaller than the size of circumbinary disk. Circumstellar disks in binary systems have been observed by many authors in the past (e.g. Mayama et al. 2010). These circumstellar disks could be other irradiation sources. We estimate their luminosities as follows: the maximum luminosity of each disk is given by $L_{\text{disk}} = GM\dot{M}_{\text{crit}}/R_* \sim 7 \times 10^{-2} L_{\odot}(M/M_{\odot})^2(R_*/R_{\odot})^{-1}$ with $\dot{M}_{\text{crit}} = L_{\text{Edd}}/c^2$, where the Eddington luminosity is given by $L_{\text{Edd}} \simeq 1.3 \times 10^{38} (M/M_{\odot}) \text{ erg s}^{-1}$. Since it is substantially smaller than the stellar luminosity, the effect of the circumstellar-disk irradiation is negligible.

Since the surface element on the circumbinary disk is given in the polar coordinates by

$$d\mathbf{S} = \frac{\partial \mathbf{r}}{\partial r} \times \frac{\partial \mathbf{r}}{\partial \phi} dr d\phi = \left[\mathbf{l} - \mathbf{r} \left(-\frac{\partial \beta}{\partial r} \sin \phi + \frac{\partial \gamma}{\partial r} \cos \phi \sin \beta \right) \right] r dr d\phi, \quad (13)$$

the radiative flux at $d\mathbf{S}$ is given by

$$dL = \frac{1}{4\pi} \sum_{i=1}^2 \frac{L_i}{|\mathbf{r} - \mathbf{r}_i|^2} \frac{|(\mathbf{r} - \mathbf{r}_i) \cdot d\mathbf{S}|}{|\mathbf{r} - \mathbf{r}_i|}, \quad (14)$$

where L is the sum of luminosities of the radiation emitted from the primary star, L_1 , and that from the secondary star, L_2 . Here, we assume that the surface element is not shadowed by other interior parts of the circumbinary disk. If we ignore limb darkening, the force acting on the disk surface by the radiation reaction has the magnitude of $(2/3)(dL/c)$ and is antiparallel to the local disk normal (Pringle 1996). The total radiative force on $d\mathbf{S}$ can then be written by

$$d\mathbf{F}_{\text{rad}} = \frac{1}{6\pi c} \sum_{i=1}^2 L_i \frac{|(\mathbf{r} - \mathbf{r}_i) \cdot d\mathbf{S}|}{|\mathbf{r} - \mathbf{r}_i|^3} \frac{d\mathbf{S}}{|d\mathbf{S}|}. \quad (15)$$

Consequently, the total radiative torque acting on a ring of radial width dr is given by

$$d\mathbf{T}_{\text{rad}} = \oint \mathbf{r} \times d\mathbf{F}_{\text{rad}} \approx \frac{L}{6\pi c r^3} \oint |\mathbf{r} \cdot d\mathbf{S}| \frac{\mathbf{r} \times d\mathbf{S}}{|d\mathbf{S}|} + \frac{1}{2\pi c r^5} \oint \sum_{i=1}^2 L_i |(\mathbf{r} - \mathbf{r}_i) \cdot d\mathbf{S}| (\mathbf{r} \cdot \mathbf{r}_i) \frac{\mathbf{r} \times d\mathbf{S}}{|d\mathbf{S}|}, \quad (16)$$

where $\oint |(\mathbf{r} - \mathbf{r}_i) \cdot d\mathbf{S}| (\mathbf{r} \times d\mathbf{S}) / |d\mathbf{S}| = \oint |\mathbf{r} \cdot d\mathbf{S}| (\mathbf{r} \times d\mathbf{S}) / |d\mathbf{S}|$ holds for $\beta \ll 1$ and $r\partial\beta/\partial r \ll 1$, and the first term, which we call $d\mathbf{T}_0$, of the right-hand side of equation (16) corresponds to equation (2.15) of Pringle (1996):

$$d\mathbf{T}_0 = \frac{L}{6c} \left(r \frac{\partial l_y}{\partial r} \mathbf{i} - r \frac{\partial l_x}{\partial r} \mathbf{j} \right) dr \quad (17)$$

and the second term, which we call $d\mathbf{T}_{\text{orb}}$, is originated from the orbital motion of the binary.

Here, we consider the radiation-driven warping/precession with timescales much longer than the orbital period, as in the case of tidally driven warping/precession. The orbit-average of the torque $d\mathbf{T}_{\text{rad}}$ is then given by

$$\begin{aligned} \langle d\mathbf{T}_{\text{rad}} \rangle &= \frac{1}{2\pi} \int_0^{2\pi} d\mathbf{T}_{\text{rad}} d(\Omega_{\text{orb}} t) \approx d\mathbf{T}_0 + \frac{1}{2\pi} \int_0^{2\pi} d\mathbf{T}_{\text{orb}} d(\Omega_{\text{orb}} t) \\ &= \frac{L}{6c} \left\{ \left(-\frac{3}{2} \zeta(1 - e^2) \left(\frac{a}{r} \right)^2 l_y + r \left[1 - \frac{3}{8} \zeta(4 + e^2) \left(\frac{a}{r} \right)^2 \right] \frac{\partial l_y}{\partial r} \right) \mathbf{i} \right. \\ &\quad \left. + \left(\frac{3}{2} \zeta(1 + 4e^2) \left(\frac{a}{r} \right)^2 l_x - r \left[1 - \frac{3}{8} \zeta(4 + 11e^2) \left(\frac{a}{r} \right)^2 \right] \frac{\partial l_x}{\partial r} \right) \mathbf{j} \right\} dr, \quad (18) \end{aligned}$$

where $\zeta \equiv (\xi_1^2 L_1 + \xi_2^2 L_2)/L$ is a binary irradiation parameter ($\zeta < 1$ by definition), and $\langle d\mathbf{T}_{\text{rad}} \rangle$ is reduced to $d\mathbf{T}_0$ for $r \gg a$.

From equation (18), the specific radiative torque averaged over azimuthal angle and orbital phase is given by

$$\begin{aligned} \langle \mathbf{T}_{\text{rad}} \rangle &= \frac{1}{2\pi r \Sigma} \frac{\langle d\mathbf{T}_{\text{rad}} \rangle}{dr} = |\mathbf{J}| \frac{\Gamma}{r} \left\{ \left(-\frac{3}{2} \zeta (1 - e^2) \left(\frac{a}{r} \right)^2 l_y + r \left[1 - \frac{3}{8} \zeta (4 + e^2) \left(\frac{a}{r} \right)^2 \right] \frac{\partial l_y}{\partial r} \right) \mathbf{i} \right. \\ &+ \left. \left(\frac{3}{2} \zeta (1 + 4e^2) \left(\frac{a}{r} \right)^2 l_x - r \left[1 - \frac{3}{8} \zeta (4 + 11e^2) \left(\frac{a}{r} \right)^2 \right] \frac{\partial l_x}{\partial r} \right) \mathbf{j} \right\}, \end{aligned} \quad (19)$$

where $\Gamma = L/(12\pi\Sigma r^2\Omega c)$ and Σ are the growth speed of a warping mode induced by the radiative torque and disk surface density, respectively. The growth timescale of the warping mode for an optically thick gas disk can be estimated to be

$$\tau_{\text{rad}} = \frac{r}{\Gamma} = 6GM\Sigma \left(\frac{c}{L} \right) \left(\frac{r}{a} \right)^{3/2} P_{\text{orb}} = 6.2 \times 10^3 \left(\frac{r}{a} \right)^{3/2} \left(\frac{\Sigma}{1 \text{ g cm}^{-2}} \right) \left(\frac{M}{M_{\odot}} \right) \left(\frac{L}{L_{\odot}} \right)^{-1} P_{\text{orb}}. \quad (20)$$

Since it is clear that the growth timescale for $r > a$ is much longer than the orbital period, our assumption for the orbit-averaged radiative torque is ensured.

3. Tilt angle evolution of circumbinary disks

In this section, we examine the response of the circumbinary disk to the external forces for $\beta \ll 1$ case. The evolution equation for disk tilt is given by (Pringle 1996)

$$\frac{\partial \mathbf{l}}{\partial t} + \left[v_r - \nu_1 \frac{\Omega'}{\Omega} - \frac{1}{2} \nu_2 \frac{(r^3 \Omega \Sigma)'}{r^3 \Omega \Sigma} \right] \frac{\partial \mathbf{l}}{\partial r} = \frac{\partial}{\partial r} \left(\frac{1}{2} \nu_2 \frac{\partial \mathbf{l}}{\partial r} \right) + \frac{1}{2} \nu_2 \left| \frac{\partial \mathbf{l}}{\partial r} \right|^2 \mathbf{l} + \mathbf{T}_{\text{ex}}, \quad (21)$$

where ν_1 and ν_2 are respectively the horizontal and vertical shear viscosities, the latter of which tends to reduce disk tilt, and \mathbf{T}_{ex} is the term to which the external torques contribute. For a geometrically thin disk, ν_1 is approximately given by $\nu_1 \approx \alpha c_s^2 / \Omega = \alpha (R_g / \mu) T / \Omega$ with the Shakura-Sunyaev viscosity parameter α (Shakura & Sunyaev 1973), the isothermal sound speed c_s , the temperature T , the gas constant R_g , and the molecular weight μ .

The primes indicate differentiation with respect to r . We adopt for the circumbinary disk structure the following assumptions that $v_r = \nu_1 \Omega' / \Omega$,

$$\Sigma(r) = \Sigma_0 \left(\frac{r}{r_0} \right)^n \quad (n < 0), \quad (22)$$

$$T(r) = T_0 \left(\frac{r}{r_0} \right)^s \quad (s < 0), \quad (23)$$

where n and s are a constant, and r_0 , Σ_0 , and T_0 are the fiducial radius, fiducial surface density, and fiducial temperature, respectively. Equation (21) can be then reduced to

$$\frac{\partial \mathbf{l}}{\partial t} = \frac{1}{2} \nu_2 \frac{\partial^2 \mathbf{l}}{\partial r^2} + \frac{1}{2} (n + s + 3) \frac{\nu_2}{r} \frac{\partial \mathbf{l}}{\partial r} + \mathbf{T}_{\text{ex}}, \quad (24)$$

where $\mathbf{l} \cdot \partial \mathbf{l} / \partial r = 0$ is used. Here, $\nu_2 \equiv \eta \nu_1 \approx \eta \alpha (R_g / \mu) (T(r) / \Omega)$ with the ratio of vertical to horizontal viscosities: $\eta = \nu_2 / \nu_1$ and \mathbf{T}_{ex} is written as

$$\begin{aligned} \mathbf{T}_{\text{ex}} &= (\langle \mathbf{T}_{\text{grav}} \rangle + \langle \mathbf{T}_{\text{rad}} \rangle) / |\mathbf{J}| \\ &= \left\{ \frac{3}{2} \left(\frac{a}{r} \right)^2 (1 - e^2) \left[\frac{1}{2} \xi_1 \xi_2 \Omega - \frac{\zeta}{\tau_{\text{rad}}} \right] l_y + \Gamma \left[1 - \frac{3}{8} \zeta \left(\frac{a}{r} \right)^2 (4 + e^2) \right] \frac{\partial l_y}{\partial r} \right\} \mathbf{i} \\ &\quad - \left\{ \frac{3}{2} \left(\frac{a}{r} \right)^2 (1 + 4e^2) \left[\frac{1}{2} \xi_1 \xi_2 \Omega - \frac{\zeta}{\tau_{\text{rad}}} \right] l_x + \Gamma \left[1 - \frac{3}{8} \zeta \left(\frac{a}{r} \right)^2 (4 + 11e^2) \right] \frac{\partial l_x}{\partial r} \right\} \mathbf{j}. \end{aligned} \quad (25)$$

We look for solutions of equation (24) of the form $l_x, l_y \propto \exp i(\omega t + kr)$ with $kr \ll 1$. Replacing $\partial / \partial t$ with $i\omega$, $\partial / \partial r$ with ik , and $\partial^2 / \partial r^2$ with $-k^2$, we have the following set of linearized equations:

$$\begin{bmatrix} i\omega + \nu_2 k^2 / 2 - (ik/2)(n + s + 3)(\nu_2 / r) & -(\mathcal{A} + ik\mathcal{B}) \\ (\mathcal{C} + ik\mathcal{D}) & i\omega + \nu_2 k^2 / 2 - (ik/2)(n + s + 3)(\nu_2 / r) \end{bmatrix} \begin{pmatrix} l_x \\ l_y \end{pmatrix} = 0, \quad (26)$$

where

$$\begin{aligned} \mathcal{A} &= (1 - e^2) \Omega_{\text{p,circ}}, \\ \mathcal{B} &= \Gamma \left[1 - \frac{3}{8} \zeta \left(\frac{a}{r} \right)^2 (4 + e^2) \right], \\ \mathcal{C} &= (1 + 4e^2) \Omega_{\text{p,circ}}, \\ \mathcal{D} &= \Gamma \left[1 - \frac{3}{8} \zeta \left(\frac{a}{r} \right)^2 (4 + 11e^2) \right], \end{aligned} \quad (27)$$

and, $\Omega_{\text{p,circ}}$ represents the magnitude of the local precession frequency of the liner warping mode for the case of the standard disk model and $e = 0$ (see equation (35) of Paper I):

$$\Omega_{\text{p,circ}} = \frac{3}{2} \left(\frac{a}{r}\right)^2 \left[\frac{1}{2} \xi_1 \xi_2 \Omega - \frac{\zeta}{\tau_{\text{rad}}} \right]. \quad (28)$$

The determinant of the coefficient matrix on the left hand side of equation (26) must vanish because of $\mathbf{l} \neq 0$. The local dispersion relation is then obtained as

$$\omega = i \left[\frac{\nu_2 k^2}{2} \pm \frac{1}{\sqrt{2}} (\sqrt{X^2 + Y^2} - X)^{1/2} \right] \pm \frac{1}{\sqrt{2}} (\sqrt{X^2 + Y^2} + X)^{1/2}, \quad (29)$$

where

$$\begin{aligned} X &= \mathcal{AC} - k^2 \mathcal{BD} \approx (1 + 3e^2) \Omega_{\text{p,circ}}^2 - (k\Gamma)^2 \left[1 - 3\zeta \left(1 + \frac{3}{2} e^2 \right) \left(\frac{a}{r} \right)^2 \right], \\ Y &= \mathcal{AD} + \mathcal{BC} \approx -2k\Gamma \Omega_{\text{p,circ}} \left[\left(1 + \frac{3}{2} e^2 \right) - \frac{3}{2} \zeta (1 + 3e^2) \left(\frac{a}{r} \right)^2 \right], \\ X^2 + Y^2 &\approx \left\{ (1 + 3e^2) \Omega_{\text{p,circ}}^2 + (k\Gamma)^2 \left[1 - 3\zeta \left(1 + \frac{3}{2} e^2 \right) \left(\frac{a}{r} \right)^2 \right] \right\}^2. \end{aligned} \quad (30)$$

Here, we adopt the approximation that the terms proportional to $(r/a)^4$ or e^4 are negligible in comparison with the other terms. The dispersion relation is then rewritten in the following simple form:

$$\omega = i \left\{ \frac{\nu_2 k^2}{2} \pm k\Gamma \left[1 - 3\zeta \left(1 + \frac{3}{2} e^2 \right) \left(\frac{a}{r} \right)^2 \right]^{1/2} \right\} \pm \sqrt{1 + 3e^2} \Omega_{\text{p,circ}} + \frac{1}{2} \frac{k\nu_2}{r} (n + s + 3) \quad (31)$$

The imaginary part of ω corresponds to the excitation or damping of oscillation, whereas the real part provides the local precession frequency due to the external torques.

In order for the perturbation to grow, $\text{Im}(\omega)$ must be negative. The growth condition is given by

$$0 < k < \frac{2\Gamma}{\nu_2} \left[1 - 3\zeta \left(1 + \frac{3}{2} e^2 \right) \left(\frac{a}{r} \right)^2 \right]^{1/2}. \quad (32)$$

In terms of $\Gamma_{\text{bin}} \equiv \Gamma [1 - 3\zeta (1 + 3e^2/2) (a/r)^2]^{1/2}$, the growth timescale of the warping mode induced by the radiative torques in the binary system is given by

$$\tau_{\text{rad,bin}} = \frac{r}{\Gamma_{\text{bin}}} = \tau_{\text{rad}} \left[1 - 3\zeta \left(1 + \frac{3}{2} e^2 \right) \left(\frac{a}{r} \right)^2 \right]^{-1/2}. \quad (33)$$

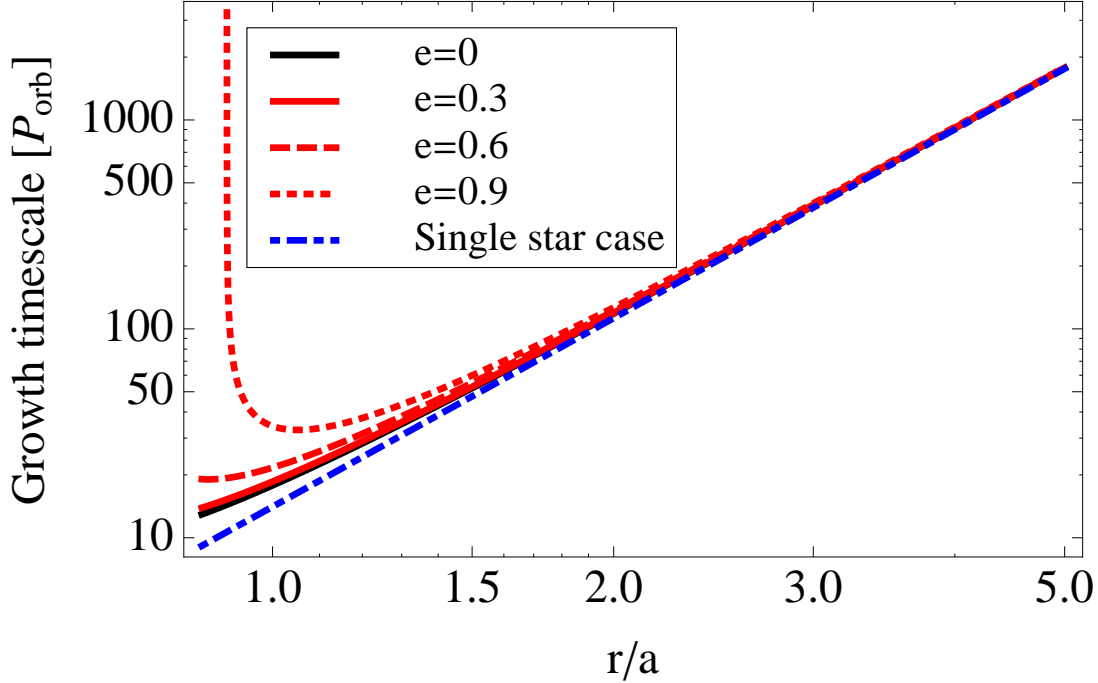


Fig. 2.— Growth timescale of the radiation-driven warping of a circumbinary disk. Here we adopted that $\zeta = 1/4$ ($q = 1$), $\Sigma = 1 \text{ g cm}^{-2}$, $L = 10^4 L_{\odot}$, $M = 30 M_{\odot}$, and $a = 1 \text{ AU}$. Each growth timescale is normalized by $P_{\text{orb}} \simeq 67$ days. The black solid, red solid, red dashed, and red dotted lines show the growth timescales for the orbital eccentricity $e = 0.0, 0.3, 0.6$, and 0.9 , respectively. The blue dot-dashed line corresponds to that of the single star case.

Figure 2 shows the dependence of $\tau_{\text{rad,bin}}$ on the orbital eccentricity and r/a in a circumbinary disk with $\zeta = 1/4$ ($q = 1$), $\Sigma = 1 \text{ g cm}^{-2}$, $L = 10^4 L_{\odot}$, $M = 30 M_{\odot}$, and $a = 1 \text{ AU}$. Each growth timescale is normalized by $P_{\text{orb}} \simeq 67$ days. The growth timescale is longer than that of circular binary case in the range of $r/a < 3$. This is because the averaged incident flux normal to the disk surface per binary orbit is lower than that of the circular binary case. Note that $\tau_{\text{bin,rad}}$ is approximately equal to τ_{rad} for $r/a \geq 3$. We therefore treat τ_{rad} as the growth timescale of the binary star case in what follows.

We focus our attention on a perturbation with $\lambda \leq r$, where $\lambda = 2\pi/k$ is the radial wavelength of the perturbation. The condition that the circumbinary disk is unstable to the warping mode can be, then, rewritten as

$$r \leq \frac{1}{12\pi^2\eta\alpha\Sigma c_s^2} \left(\frac{L}{c}\right) \left[1 - 3\zeta \left(1 + \frac{3}{2}e^2\right) \left(\frac{a}{r}\right)^2\right]^{1/2}. \quad (34)$$

Substituting equations (22) and (23) into the above equation, we obtain

$$\frac{r}{r_0} \begin{cases} \geq (r_{\text{warp}}/r_0) \left[1 - 3\zeta \left(1 + \frac{3}{2}e^2\right) \left(\frac{a}{r}\right)^2\right]^{1/(2(n+s+1))} & (n + s + 1 < 0) \\ \leq (r_{\text{warp}}/r_0) \left[1 - 3\zeta \left(1 + \frac{3}{2}e^2\right) \left(\frac{a}{r}\right)^2\right]^{1/(2(n+s+1))} & (n + s + 1 > 0), \end{cases} \quad (35)$$

where r_{warp} shows the marginally stable warping radius for a single star case:

$$\frac{r_{\text{warp}}}{r_0} = \left[12\pi^2\eta\alpha r_0 \Sigma_0 \frac{R_g}{\mu} T_0 \frac{c}{L}\right]^{-1/(n+s+1)} \approx \left[6\pi^2 \frac{1}{\alpha} r_0 \Sigma_0 \frac{R_g}{\mu} T_0 \frac{c}{L}\right]^{-1/(n+s+1)}, \quad (36)$$

where in deriving the second equation, we have used the relationship between η and α : $\eta = 2(1+7\alpha^2)/(\alpha^2(4+\alpha^2)) \approx 1/(2\alpha^2)$ for $\alpha \ll 1$ (Ogilvie 1999). In the case of $n+s+1 = 0$, no unstable solution exists except for very special combination of parameters.

The radiative torques work only for a region of optically thick to irradiation emitted from the central stars. In order for the circumbinary disk to be optically thick, the surface density must be higher than $\Sigma_{\text{min}} \simeq 1 \text{ g cm}^{-2}$, where the electron scattering opacity is assumed for simplicity. This condition is rewritten as

$$\frac{r}{r_0} \leq \left(\frac{\Sigma_{\text{min}}}{\Sigma_0}\right)^{1/n}, \quad (37)$$

using equation (22). The equality is held at the radius where the circumbinary disk changes from optically thick to optically thin:

$$\frac{r_{\text{op}}}{r_0} = \left(\frac{\Sigma_{\text{min}}}{\Sigma_0}\right)^{1/n}. \quad (38)$$

In order for radiation-driven warping to be a possible mechanism for disk warping, the marginally stable warping radius must be less than the outer radius of the optically thick

region, r_{op} . This gives the upper (lower) limit of Σ_0 for $n + s + 1 < 0$ ($n + s + 1 > 0$) as follows:

$$\Sigma_0 \begin{cases} \leq \Sigma_{\text{crit}} \left[1 - 3\zeta \left(1 + \frac{3}{2}e^2 \right) \left(\frac{a}{r} \right)^2 \right]^{-n/(2(s+1))} & (n + s + 1 < 0) \\ \geq \Sigma_{\text{crit}} \left[1 - 3\zeta \left(1 + \frac{3}{2}e^2 \right) \left(\frac{a}{r} \right)^2 \right]^{-n/(2(s+1))} & (n + s + 1 > 0), \end{cases} \quad (39)$$

where Σ_{crit} is the critical surface density given by

$$\Sigma_{\text{crit}} = \Sigma_{\text{min}}^{(n+s+1)/(s+1)} \left[12\pi^2 \eta \alpha r_0 \frac{R_g}{\mu} T_0 \frac{c}{L} \right]^{n/(s+1)}. \quad (40)$$

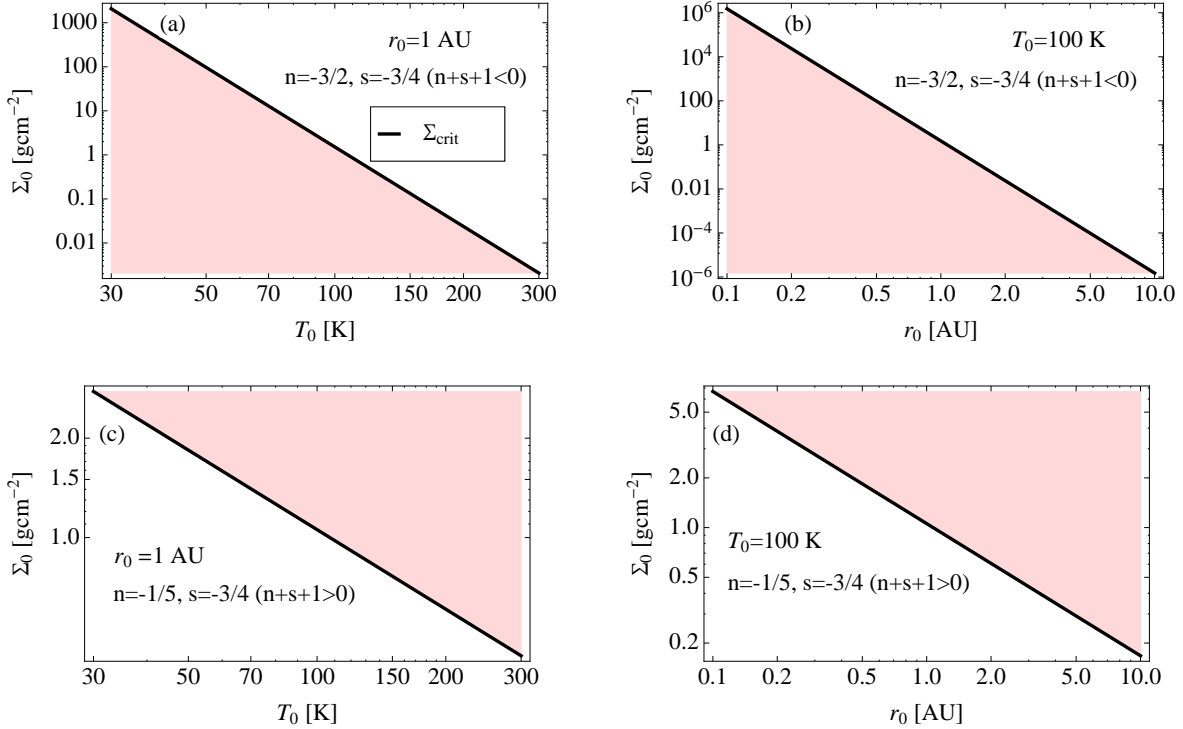


Fig. 3.— Possible range in Σ_0 (shaded area), for the circumbinary disk to be unstable to warping modes, as a function of T_0 and r_0 in the case of $r \gg a$. The black line shows a critical surface density, which is given by equation (40), for $\Sigma_{\text{min}} = 1 \text{ g cm}^{-2}$, $\alpha = 0.01$, and $L = 10^4 L_\odot$. The values of n and s are annotated in each panel.

Figure 3 shows the possible range in Σ_0 , for the circumbinary disk to be unstable to warping modes, as a function of T_0 and r_0 . The upper two panels give the range for $n + s + 1 < 0$ case, whereas the lower two panels for $n + s + 1 > 0$ case. From the figure, we can express Σ_0 as

$$\Sigma_0 = f \Sigma_{\text{crit}} \left[1 - 3\zeta \left(\frac{a}{r} \right)^2 \left(1 + \frac{3}{2} e^2 \right) \right]^{-n/(2(s+1))} \quad (41)$$

with a factor f in the range $0 < f \leq 1$ for $n + s + 1 < 0$ and $f > 1$ for $n + s + 1 > 0$. Substituting equation (41) into equation (36) with equation (35), we can obtain the marginally stable warping radius as

$$r_{\text{warp,bin}} = r_{\text{warp}} \left[1 - 3\zeta \left(1 + \frac{3}{2} e^2 \right) \left(\frac{a}{r} \right)^2 \right]^{1/(2(s+1))}, \quad (42)$$

where r_{warp} can be rewritten as

$$\begin{aligned} r_{\text{warp}} &= f^{-1/(n+s+1)} \left[6\pi^2 \frac{1}{\alpha} r_0 \Sigma_{\text{min}} \frac{R_{\text{g}}}{\mu} T_0 \frac{c}{L} \right]^{-1/(s+1)} r_0 \simeq 10^{-4/(s+1)} [\text{AU}] \left(\frac{1}{f} \right)^{1/(n+s+1)} \\ &\times \left[\left(\frac{\alpha}{0.01} \right) \left(\frac{r_0}{1 \text{ AU}} \right)^s \left(\frac{\Sigma_{\text{min}}}{1 \text{ g cm}^{-2}} \right)^{-1} \left(\frac{T_0}{100 \text{ K}} \right)^{-1} \left(\frac{L}{L_{\odot}} \right) \right]^{1/(s+1)}. \end{aligned} \quad (43)$$

Adopting for equation (43) $s = -3/4$, which corresponds to the power law index of the radial temperature profile of an optically thick region in the standard disk (Shakura & Sunyaev 1973), the marginally stable warping radius is very sensitive to the values of α , r_0 , Σ_{min} , T_0 , and L . It is clear from equations (42) and (43) that a circumbinary disk around young binary stars with $M \sim 1 M_{\odot}$ and $L \sim 1 L_{\odot}$ is stable for radiation driven warping, because the marginally stable warping radius is of the order of 10^{-16} AU for $s = -3/4$ and of 10^{-8} AU even for $s = -1/2$. This shows that the circumbinary disks of a classical T Tauri star system such as GG Tau (Dutrey et al. 1994) and UY Aurigae (Duvert et al. 1998) are not warped by radiation-driven warping instability.

On the other hand, it is likely that a circumbinary disk around binary stars with much larger luminosities is unstable to radiation-driven warping. Figure 4 shows the dependence

of the marginally stable warping radius in such a disk on the semi-major axis. Here, we adopt $\alpha = 0.01$, $s = -3/4$, $e = 0.6$, $\zeta = 1/4$ ($q = 1$), $\xi_1\xi_2 = 1/4$ ($q = 1$), $\gamma = \pi/4$, $T_0 = 100$ K, $\Sigma_{\min} = 1$ g cm $^{-2}$, $M = 30 M_{\odot}$, and $L = 10^4 L_{\odot}$. While panels (a) and (c) are for $r_0 = 1$ AU, panels (b) and (d) are for $r_0 = 0.1$ AU. We also adopt $f = 0.5$ and $n = -3/2$ in panels (a) and (b), and $f = 1$ and $n = -1/5$ in panels (c) and (d). In these four panels, the black solid line and orange dashed line show $r_{\text{warp,bin}}$ and r_{op} in units of AU, respectively. The red dotted line shows the radius where the growth timescale of the radiation-driven warping mode, τ_{rad} , equals the timescale for the disk to align with the orbital plane by the tidal torque, τ_{tid} . This tidal alignment radius is given by

$$r_{\text{rad/tid}} = \left\{ 9\pi GM\Sigma_0 \left(\frac{c}{L} \right) \xi_1\xi_2 \sqrt{5e^2(3e^2 + 2) \cos^2 \gamma + (e^2 - 1)^2} \right\}^{1/(2-n)} \left(\frac{a}{r_0} \right)^{2/(2-n)} r_0, \quad (44)$$

from equations (12), (20) and (22). The growth of a finite-amplitude warping mode induced by the radiative torque can be significantly suppressed by the tidal torque in the region inside the tidal alignment radius. The blue dot-dashed line show the inner radius of the circumbinary disk. Here, the inner radius is assumed to be equal to the tidal/resonant truncation radius, where the tidal/resonant torque is balanced with the horizontal viscous torque of the circumbinary disk (Artymowicz & Lubow 1994). In the case of eccentric binaries with a nearly equal mass ratio, the tidal/resonant truncation radius is estimated to be $\sim 2a$. The shaded area shows the region where the circumbinary disk is unstable to the warping modes induced by the radiative torques.

From the figure, the marginally stable warping radius is on a sub-AU to kilo-AU scale for appropriate model parameters. In panes (a) and (b), the circumbinary disk is warped in the region outside all of the marginally stable warping radius, the tidally alignment radius, and the inner disk radius, and inside the outer radius of the optically thick part (in the region above the black line, below the orange dashed line, and on the left-side of both the red dotted line and the blue dot-dashed line). On the other hand, in panels (c) and (d), the

circumbinary disk is warped in the region inside both the marginally stable warping radius and the outer radius of the optically thick region, and outside both the tidal alignment radius and the inner disk radius (in the region below the black line and the orange dashed line, and on the left-side of both the red dotted line and the blue dot-dashed line). Note that in any case the middle part of the circumbinary disk is warped because the warping mode in the inner part is suppressed by the tidal torques, and the radiative torques are effective only within the outer radius of the optically thick region.

The local precession frequency $\Omega_{\text{p,tot}}$ of the linear warping mode is obtained from the dispersion relation by

$$\Omega_{\text{p,tot}} = \Omega_{\text{p,tid}} + \Omega_{\text{p,rad}} + \Omega_{\text{p,vis}}, \quad (45)$$

where

$$\Omega_{\text{p,tid}} = -\frac{3}{4}\xi_1\xi_2\sqrt{1+3e^2}\left(\frac{a}{r}\right)^{7/2}\Omega_{\text{orb}}, \quad (46)$$

$$\Omega_{\text{p,rad}} = \frac{3}{2}\zeta\sqrt{1+3e^2}\left(\frac{a}{r}\right)^2\frac{1}{\tau_{\text{rad}}}, \quad (47)$$

$$\Omega_{\text{p,vis}} = \frac{k\nu_2}{2r}(n+s+3), \quad (48)$$

where $\Omega_{\text{p,tid}}$, $\Omega_{\text{p,vis}}$, $\Omega_{\text{p,rad}}$ are the local precession frequencies due to the tidal, viscous, and radiative torques, respectively. Note that $\Omega_{\text{p,tid}}$ has the same expression with the opposite sign to the precession frequency of the tidally induced $m = 1$ wave (see equation (11) of Hayasaki & Okazaki 2009). This satisfies the condition for simultaneous resonant excitation of eccentric and tilt waves proposed by Kato (2014). Therefore, both waves are likely to coexist in the circumbinary disk.

Adopting $k \leq (2\Gamma/\nu_2)\sqrt{1-3\zeta(a/r)^2(1+(3/2)e^2)}$ from equation (32), we obtain

$$\Omega_{\text{p,tot}} \lesssim -\frac{3}{2}\sqrt{1+3e^2}\left(\frac{a}{r}\right)^2\left[\frac{1}{2}\xi_1\xi_2\Omega + (n+s+2)\frac{\zeta}{\tau_{\text{rad}}}\right] + \frac{n+s+3}{\tau_{\text{rad}}}, \quad (49)$$

While the circumbinary disk tends to precess in the retrograde direction by the tidal torques, it tends to precess in the prograde direction by the other two torques. Figure 5

shows the radial dependence of the precession timescales. The black solid line, the red dashed line, the orange dot-dashed line, and the blue dotted line show the precession timescale for the radiative torques $\tau_{p,\text{rad}} = 1/\Omega_{p,\text{rad}}$, tidal torques $\tau_{p,\text{tid}} = 1/\Omega_{p,\text{tid}}$, viscous torque due to vertical shear $\tau_{p,\text{vis}} = 1/\Omega_{p,\text{vis}}$, and total torque $\tau_{p,\text{tot}} = 1/\Omega_{p,\text{tot}}$, respectively. Each precession timescale is normalized by the orbital period. The precession timescale is much longer than the orbital period for $r/a \gg 1$. The circumbinary disk slowly precesses in the retrograde direction in the range of $r_{\text{in}}/a \leq r/a \leq 100$, because $\tau_{p,\text{tid}}$ is shorter than the other two timescales.

4. Summary and Discussion

We have investigated the instability of a warping mode in a geometrically thin, non-self-gravitating circumbinary disk induced by radiative torques originated from two young stars in a binary on an eccentric orbit. For simplicity, they have been regarded as point irradiation sources. We have formulated the external torques acting on such a circumbinary disk, which are composed of both the tidal torques due to a time-dependent binary potential and the radiative torques. Based on these formulations, we have derived the warping mode induced by the radiative torques and compared the timescales of precession caused by tidal, viscous, and radiative torques for a small tilt angle. We have found that there is a marginally stable warping radius within or beyond which the circumbinary disk is unstable to radiation-driven warping, depending on the disk density and temperature gradient indices. Our main conclusions other than this instability condition are summarized as follows:

1. The marginally stable warping radius is sensitive to the viscosity parameter (α), the surface density measured at the radius where the disk changes from the optically thick to thin (Σ_{min}), a fiducial radius (r_0), the disk temperature at r_0 (T_0), and

the stellar luminosity (L) [equation (44)], whereas it weakly depends on the orbital eccentricity and binary irradiation parameter, which is a function of binary mass ratio and luminosity of each star [equation (43)]. The marginally stable radius is on a sub-AU to kilo-AU scale for $\alpha = 0.01$, $\Sigma_{\min} = 1 \text{ g cm}^{-2}$, $T_0 = 100 \text{ K}$, $M = 30 M_{\odot}$ and $10^4 L_{\odot}$, while it is much smaller than the stellar radius for $M = 1 M_{\odot}$ and $L = 1 L_{\odot}$. The radiation-driven warping can, therefore, be a plausible mechanism for a warped structure of a circumbinary disk around a young massive binary, whereas it is an unlikely mechanism for that around a young low-mass binary.

2. There is a clear difference in the warping radius between the single star case and the binary star case. Since the tidal torques work on the circumbinary disk so as to align the disk plane with the binary orbital plane, they can suppress finite-amplitude warping modes induced by the radiative torques. The circumbinary disk, therefore, starts to be warped at the tidal alignment radius where the growth timescale of the radiation-driven warping is equal to the timescale of the disk alignment due to tidal torques, if the tidal alignment radius is larger than the marginally stable warping radius. In contrast, the circumstellar disk around a single star starts to be warped in the region beyond the marginally stable warping radius.
3. The circumbinary disk precesses by tidal torque, radiative, and vertical viscous torques. While the radiative and vertical viscous torques tend to precess the circumbinary disk in the prograde direction, the tidal torques tend to precess it in the retrograde direction. Since the former two precession frequencies are substantially lower than the latter precession frequency, the circumbinary disk slowly precesses in the retrograde direction. The precession timescale is much longer than the orbital period for the outer part of the circumbinary disk ($r/a \gtrsim 4$). Therefore, it is unlikely that the periodic light variation due to the precession of the warped disk could be

detected.

4. The tidal torques with a small tilt angle depend on the azimuth of the tilt for $e \neq 0$, whereas they have no such dependence for $e = 0$.
5. The higher the orbital eccentricity, the longer the growth timescale of radiation-driven warping mode and the shorter its precession timescale. The effect is, however, significant only in the region $r/a < 2$. For $r/a \gtrsim 3$, the growth timescale of the warping mode in the binary star case is reduced to that of the single star case.

For simplicity, we have assumed that the circumbinary disk is initially aligned with the binary orbital plane ($\beta \ll 1$), as in most of the previous studies. However, the angular momentum vector of the circumbinary disk does not always coincide with that of the binary orbital angular momentum, because the orientation of the circumbinary disk is primarily due to the angular momentum of material accreted after the binary has formed. Therefore, the orientation of the circumbinary disk plane can be taken arbitrarily with respect to the binary orbital plane. In a misaligned system with a significant tilt angle, the inner part of the circumbinary disk tends to align with the binary orbital plane by the tidal interaction between the binary and the circumbinary disk, whereas the outer part tends to retain the original state by the shear viscosity in the vertical direction. As a result, the circumbinary disk should be warped without the effect of radiation driven warping instability (e.g., Facchini et al. 2013; Lodato&Facchini 2013; Foucart&Lai 2014). It is important to examine how the radiation driven warping instability works in the misaligned systems under the tidal potential, but it is difficult to find the analytic solutions because of the complicated dependence of the tidal and radiative torques on the tilt angle and azimuth of tilt. We will numerically study this problem in the future.

There is a cavity between the circumbinary disk and the binary for a nearly equal mass to moderate mass ratio (see Figure 1) (Artymowicz & Lubow 1994). In the case of an

extreme mass ratio ($q \ll 1$), however, the material accretes through the cavity and therefore the circumbinary disk cannot maintain its cavity any longer because of significantly weaker tidal torque than in a moderate mass ratio binary. In such a situation, the system is composed of two circumstellar disks around individual young stars: a substantially larger accretion disk around the more massive, primary star (the primary disk) and a smaller accretion disk around the less massive, secondary star (the secondary disk), although there are some observational cases, in which the secondary disk is more massive than the primary disk (Akeson & Jensen 2014). In the system, the tidal torque of the secondary star tends to align the outer part of the primary disk with the orbital plane. Since the primary disk is unstable to radiation-driven warping beyond/within the marginally stable warping radius, only the outer/inner part of the primary disk is warped. Note that the marginally stable warping radius is smaller than the stellar radius for binaries with young low-mass stars with $\sim 1 M_{\odot}$ and $\sim 1 L_{\odot}$ from equation (43), as far as $\Sigma_{\min} \geq 10^{-3} \text{ g cm}^{-2}$, or, the disk opacity to the irradiation from the two stars less than $10^3 \text{ cm}^2 \text{ g}^{-1}$. Therefore, the discussion on the possible radiation-driven warping will be applied only to massive star cases. In addition to this, the primary disk is truncated by the tidal torque due to the secondary star. There are thus three characteristic radii in a circumstellar disk: the marginally stable warping radius, the tidal alignment radius, and the tidal truncation radius. The situation is clearly different from the circumbinary case. We will examine the warping instability in circumstellar disks in a subsequent paper.

According to the recent observations, the circumbinary and circumstellar disks in pre-main sequence binaries are likely to be composed of the inner gas disk and outer dusty disk. The dust opacity is much larger than the gas opacity in the case of the wavelength less than $100 \mu\text{m}$ (Ossenkopf & Henning 1994). If the dust opacity is more than $10^4 \text{ cm}^2 \text{ g}^{-1}$, the warping radius is comparable or larger than 1 AU even if the stellar luminosity is as low as $\sim 1 L_{\odot}$. This suggests that a circumbinary or circumstellar disk in a low-mass young binary

system could be warped by the radiative torque. Furthermore, such a dusty disk should be flared in the vertical direction (Chiang & Goldreich 1997). If this is the case, as the tilt angle locally increases, the radiative torques from the stars are stronger and hence the marginally stable warping radius is closer to the stars than in geometrically thin disk cases. We will also investigate in future the effect of radiation driven warping on circumbinary or circumstellar dusty disks.

Acknowledgments

The authors thank to the anonymous referee for fruitful comments and suggestions. K.H. is grateful to Jongsoo Kim for helpful discussions and his continuous encouragement. K.H. would also like to thank the Kavli Institute for Theoretical Physics (KITP) for their hospitality and support during the program on "A Universe of Black Holes". B.W.S. and T.H.J. are grateful for support from KASI-Yonsei DRC program of Korea Research Council of Fundamental Science and Technology (DRC-12-2-KASI). This work was also supported in part by the Grants-in-Aid for Scientific Research (C) of Japan Society for the Promotion of Science (23540271 T.N. and K.H.; 24540235 A.T.O. and K.H.).

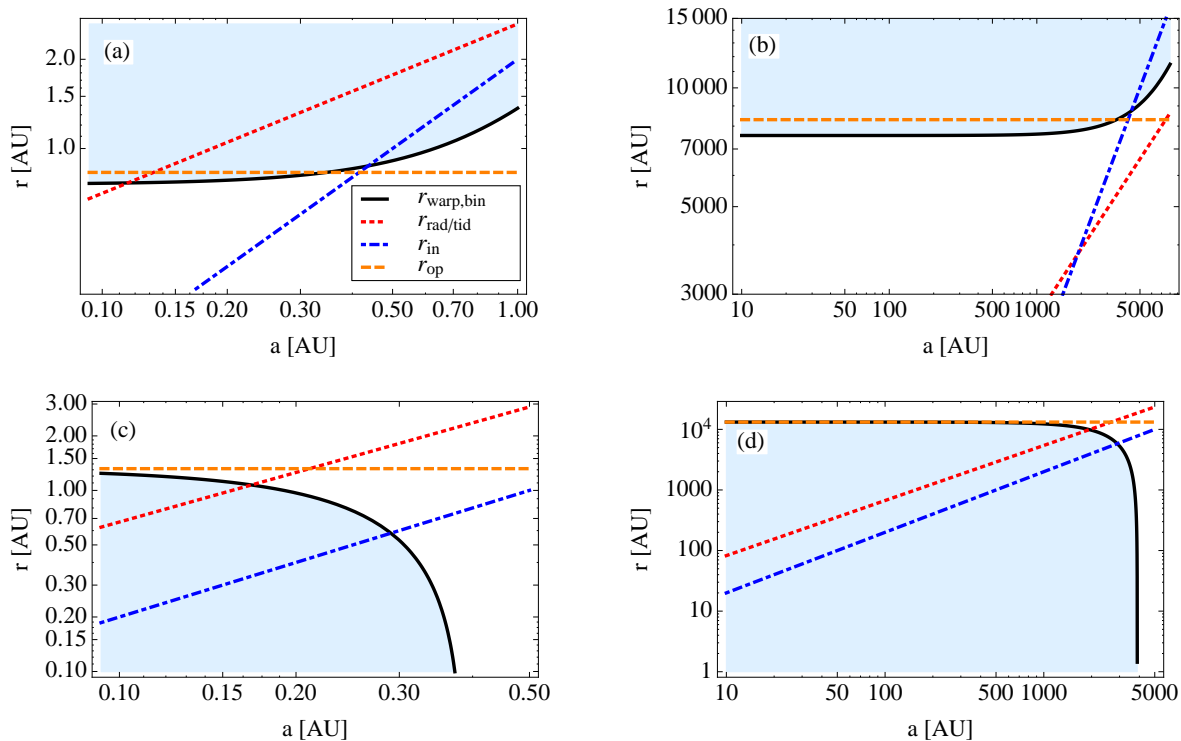


Fig. 4.— Characteristic radii of the warped circumbinary disk around young massive binaries on an eccentric orbit for $\alpha = 0.01$, $s = -3/4$, $e = 0.6$, $\zeta = 1/4$ ($q = 1$), $\xi_1 \xi_2 = 1/4$ ($q = 1$), $\gamma = \pi/4$, $T_0 = 100$ K, $\Sigma_{\min} = 1 \text{ g cm}^{-2}$, $M = 30 M_{\odot}$, and $L = 10^4 L_{\odot}$. While $r_0 = 1$ AU is adopted in panels (a) and (c), $r_0 = 0.1$ AU is adopted in panels (b) and (d). In panels (a) and (b) $f = 0.5$ and $n = -3/2$ are used, whereas $f = 1$ and $n = -1/5$ are used in panels (c) and (d). In these four panels, the black solid line shows the marginally stable warping radius of the binary star case, which is given by equation (42). The orange dashed line shows the outer radius of the optically thick region, which is given by equation (38). The red dotted line shows the tidal alignment radius where the growth timescale of the radiation-driven warping of the circumbinary disk is equal to the timescale during which the disk is aligned with the orbital plane by the tidal torques. The tidal alignment radius is given by equation (44). The blue dot-dashed line represents the inner radius of the circumbinary disk $r_{\text{in}} = 2a$.

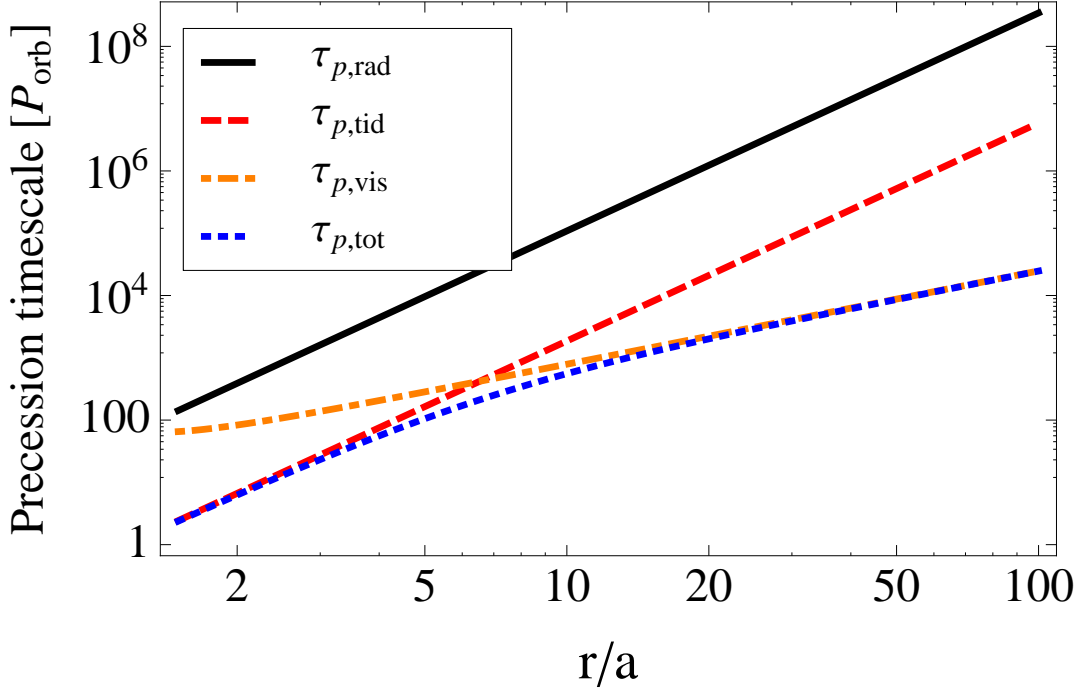


Fig. 5.— Precession timescale of the warped circumbinary disk around young massive binaries on an eccentric orbit with $e = 0.6$, $\zeta = 1/4 (q = 1)$, $\xi_1 \xi_2 = 1/4 (q = 1)$, $\Sigma = 1 \text{ g cm}^{-2}$, $n = -3/2$, $s = -3/4$, $M = 30 M_\odot$, and $a = 1 \text{ AU}$. Each precession timescale is normalized by $P_{\text{orb}} \simeq 67 \text{ days}$. The black solid line, red dashed line, orange dot-dashed line, and blue dotted line show the precession timescales from the radiative torque, from the tidal torque, from the viscous torque due to vertical shear, and from the sum of those three torques, respectively.

REFERENCES

- Akeson, R. L., & Jensen, E. L. N. 2014, *ApJ*, 784, 62
- Araya, E. D., Hofner, P., Goss, W. M., et al. 2010, *ApJ*, 717, L133
- Artymowicz, P., & Lubow, S.H. 1994, *ApJ*, 421, 651
- Artymowicz, P., & Lubow, H. S. 1996, *ApJ*, 467, L77
- Bate, M. R., & Bonnell, I. A. 1997, *MNRAS*, 285, 33
- Bate, M. R., Bonnell, I. A., Clarke, C. J., Lubow, H., Ogilvie, G. I., Pringle, J. E., & Tout, C. A. 2000, *MNRAS*, 317, 773
- Chiang, E. I., & Goldreich, P. 1997, *ApJ*, 490, 368
- Duquennoy, A. & Mayor, M. 1991, *A&A*, 248, 485
- Dutrey, A., Guilloteau, S. & Simon M. 1994, *A&A*, 286, 149
- Duvert, G., et al. 1998, *A&A*, 332, 867
- Facchini S., Lodato G., & Price D. J., 2013, *MNRAS*, 433, 2142
- Foucart, F., & Lai, D., 2014 arXiv:1406.3331
- Günther, R. C., & Kley, W. 2002, *A&A*, 387, 550
- Günther, R. C & Kley, W. 2004, *A&A*, 423, 559
- Hayasaki, K., & Okazaki, A.T. 2009, *ApJ*, 691, L5
- Hayasaki, K., Sohn, B. W., Okazaki, A., Jung, T., Zhao, G., Naito T. 2014, *ApJ*, 70, 62
(Paper I)

- Hayasaki, K., Sohn, B. W., Okazaki, A., Jung, T., Zhao, G., Naito T. 2014, submitted to MNRAS
- Hilditch, R. W., Howarth, I. D., & Harries, T. J. 2005, MNRAS, 357, 304
- Inayoshi K., Sugiyama K., Hosokawa T., Motogi K., & Tanaka K. E. I. 2013, ApJ, 769, L20
- Kato, S. 2014, PASJ, in press (arXiv:1405.3372)
- Kormendy, J., & Ho, L. C. 2013, ARA&A, 51, 511
- Krist, J. E., Stapelfeldt, K. R., Golimowski, D. A., et al. 2005, AJ, 130, 2778
- Kuo, C. Y., Braatz, J. A., Condon, J. J., Impellizzeri, C. M. V., Lo, K. Y., Zaw, I., Schenker, M., Henkel, C., Reid, M. J., & Greene, J. E. 2011, ApJ, 727, 20
- Lodato, G. & Facchini, S. 2013, MNRAS, 433, 2157
- Mathieu, R. D., Latham, D. W., & Griffin, R. F. 1990, AJ, 100, 1859
- Mayama, S., Tamura, M., Hanawa, T., et al. 2010, Science, 327, 306
- Moeckel N., & Bally, J. 2006, ApJ, 653, 437
- Ogilvie, G. 1999, MNRAS, 304, 557
- Ossenkopf, V., & Henning, Th. 1994, A&A, 291, 943
- Pringle, J. E. 1996, MNRAS, 281, 357
- Sana, H., de Mink, S. E., de Koter, A., et al. 2012, Sci, 337, 444
- van der Walt, D. J. 2011, AJ, 141, 152
- Shakura, N. I., & Sunyaev, R. A. 1973, A&A, 24, 337